Comparative biomechanical analysis demonstrates functional convergence between slender-snouted crocodilians and phytosaurs

Robert Lemanis[1*], Andrew S. Jones[2], Richard J. Butler[2], Philip S. L. Anderson[3] and Emily J. Rayfield[4]

[1]B CUBE - Center for Molecular Bioengineering, Technische Universität Dresden, 01307, Dresden, Germany

[2]School of Geography, Earth and Environmental Sciences, University of Birmingham, Edgbaston, Birmingham, B15 2TT, United Kingdom

[3]Department of Animal Biology, University of Illinois at Urbana-Champaign, Urbana, Illinois, 61801, USA

[4]School of Earth Sciences, University of Bristol, Bristol BS8 1RJ, United Kingdom

Corresponding author:

Robert Lemanis

Tatzberg 41 18, 01307 Dresden

Email: robert_evan.lemanis@tu-dresden.de

Abstract

Morphological similarities between the extinct Triassic archosauriform clade Phytosauria and extant crocodilians have formed the basis of long-proposed hypotheses of evolutionary convergence. These hypotheses have informed the reconstructions of phytosaur ecology and biology, including feeding preferences, body mass, soft tissue systems, mating behaviours, and environmental preferences. However, phytosaurs possess numerous cranial apomorphies that distinguish them from modern crocodilians and potentially limit ecomorphological comparisons. Here, we present the first computational mechanical comparison of phytosaur cranial strength to

several extant crocodilian taxa using two biomechanical approaches: beam theory and finite element analysis. We demonstrate mechanical convergence between the slender-snouted phytosaur *Ebrachosuchus neukami* and modern slender-snouted crocodilians. We provide evidence that the phytosaurian premaxillary palate is functionally equivalent to the crocodilian secondary palate. The premaxillary palate is associated with greater resistance to biting induced stress, lower strain energy, higher resistance to bending and torsion, as well as increased performance under tension. In all tests, *Ebrachosuchus* performed worse than all tested crocodilians, showing higher stress under equivalent loading conditions. These findings have implications for the proposed feeding ecology of slender-snouted phytosaurs and corroborate previous broad assessments of phytosaur ecology based on morphological comparisons to crocodilians; however, we urge caution in overextending those assessments given the current paucity of comparative functional data.

Introduction

Phytosaurs are a near globally distributed group of extinct archosauriforms that have generally been considered the earliest branching lineage within Pseudosuchia (Fig. 1), the clade that includes modern crocodilians and their extinct stem lineage (e.g. Ezcurra, 2016). However, they have also recently been hypothesized to form the sister group to archosaurs, the major vertebrate clade that contains pseudosuchians, as well as birds, dinosaurs and pterosaurs (Nesbitt, 2011). Phytosaur fossils are commonly present throughout nearly the entire Late Triassic (late Carnian–Rhaetian; c. 232–201.3 Ma) (Brusatte et al., 2013; Stocker & Butler, 2013), and have long been characterized as an exemplar of deep time evolutionary convergence (Fig. 2), based on their strong morphological similarities with modern crocodilians (e.g., McGregor, 1906; Camp, 1930; Colbert, 1947; Hunt, 1989). Three distinct skull morphotypes have been proposed to be

present in phytosaurs (Camp, 1930; Gregory, 1962; Hunt, 1989): a "slender-snouted" form (Fig. 2 B,C) with comparatively homodont dentition (e.g. *Parasuchus* spp., *Mystriosuchus planirostris*, *Ebrachosuchus neukami*, *and Nicrosaurus meyeri*), a morphologically intermediate "moderate-snouted" form (Fig 2E) (e.g. *Angistorhinus* spp. and *Leptosuchus* spp.), and a "massively-snouted" form (Fig. 2G) (e.g. *Nicrosaurus kapffi*, *Smilosuchus gregorii*), with the latter two forms showing a more heterodont dentition (Hunt, 1989; Hungerbühler, 2000). The morphology and ecology of the slender-snouted phytosaurs have been compared to the living slender-snouted crocodilians: *Gavialis gangeticus* (the Indian gharial) (Fig. 2 A,D) and *Crocodylus* (*Mecistops) cataphractus* (the African slender-snouted crocodile), whereas the other rostrum morphologies have been hypothesised as functionally analogous to other living crocodilians such as members of Alligatoroidea, and *Crocodylus niloticus* (the Nile crocodile) (Fig. 2 F,H) (Camp, 1930; Hunt, 1989; Kimmig & Arp, 2010). However, 200 million years separates the youngest phytosaur fossils from modern crocodilians. Phytosaurs are not direct ancestors of crocodilians and the common ancestor of the two groups lived more than 245 million years ago (Nesbitt, 2011; Stocker & Butler, 2013). Moreover, despite overall morphological similarities, long-recognised anatomical differences exist that potentially limit functional and ecological comparisons between the two clades.

Notably, phytosaurs lack the bony secondary palate (formed by midline fusion of the palatine bones) that forms the roof of the mouth in crocodilians and which separates the airway and oral cavity. Phytosaurs possess external nares that are located posteriorly and dorsally, behind the mid-point of the skull and immediately anterodorsal to or above the antorbital fenestrae; furthermore, the elongated rostrum is formed primarily of the premaxilla (Camp, 1930; Stocker & Butler, 2013). By contrast, the elongated rostrum of modern crocodilians is formed primarily by

71 the maxilla, the external nares of modern crocodilians are positioned at the tip of the rostrum, and
72 the antorbital fenestra is absent. These detailed anatomical differences may impact functional
73 performance, and suggest potential problems for assumptions of function justified solely upon
74 apparently analogous gross morphology. Hypotheses concerning convergent functional
75 morphology between extant crocodilians and phytosaurs (e.g., Hunt, 1989) have never been
76 tested through quantitative biomechanical analyses.

77 Here, we focus in particular on proposed similarities between slender-snouted phytosaurs
78 (using *Ebrachosuchus neukami* as our exemplar) and slender-snouted crocodilians (in particular,
79 the gharial). The bony secondary palate present in extant crocodilians such as the gharial (as well
80 as in mammals) has been shown to strengthen the skull (Thomason & Russell, 1986; Busbey,
81 1995; Rayfield et al., 2007). Although *Ebrachosuchus* lacks a true secondary palate formed by
82 the palatines, it does, like other phytosaurs, possess an elongate premaxillary palate extending
83 along much of the length of the rostrum that ventrally bounds an extensive premaxillary sinus
84 (Fig. 2B; Witmer, 1997; Butler et al., 2014; Lautenschlager & Butler, 2016). In *Ebrachosuchus*
85 the nostrils are positioned just anterior to the antorbital fenestra. As a result, the premaxillary
86 palate would not have served as a partition between the nasal and buccal cavities. Even the
87 development of a rudimentary incomplete secondary palate that does not join at the ventral
88 midline confers a biomechanical advantage in mammalian crania (Thomason & Russell, 1986).
89 Thus, both *Ebrachosuchus* and the gharial independently evolved an elongate, hollow, tubular
90 rostrum that should strengthen the rostrum against bending and torsion (Ennos, 2012).

91 Here we present the first quantitative functional comparison between these assumed
92 analogous animals, leading to a new biomechanical perspective on phytosaur palaeoecology and
93 providing further insight into the relationship between form and function in terrestrial vertebrates.
94

Material and Methods

Choice of study taxon and hypotheses to be tested

We studied the holotype (Bayerische Staatssammlung für Paläontologie und Geologie, Munich, BSPG 1931 X 501) and only known specimen of the basal (non-Mystriosuchinae) phytosaur *Ebrachosuchus neukami* from the early Late Triassic (late Carnian, c. 230 Ma) of Bavaria, southern Germany. *Ebrachosuchus* has been considered synonymous with the basal phytosaur genus *Parasuchus* (e.g., Hunt & Lucas, 1991), but recent work supports its generic validity (Butler et al., 2014; Jones & Butler, 2018). The holotype consists of a complete skull (lacking the lower jaw) that is one of the geologically oldest and best preserved of all known phytosaur specimens, although some post-mortem dorsoventral crushing has occurred, and parts of the palatal region are damaged (see below; Fig. 3; Lautenschlager & Butler, 2016). The rostrum of *Ebrachosuchus* is proportionately longer than in any other known phytosaur (preorbital length is nearly 3.9 times as long as the orbit + postorbital length; Gregory, 1962; Butler et al., 2014) and thus it epitomizes the slender-snouted phytosaur morph. We therefore used *Ebrachosuchus* as our exemplar to test hypotheses of functional convergence between slender-snouted phytosaurs and the living gharial.

In addition to the gharial, we also included in our analyses the extant crocodilian *Crocodylus* (*Mecistops*) *cataphractus*, which has a tapering rostrum rather than tubular rostrum, *Alligator mississippiensis* as an example of a broad, flat (platyrostral) morphotype, and the Nile crocodile as an example of an apex predator. Details of the specimens used are in Table 1.

We aimed to test the following hypotheses:

(1) Does the skull of *Ebrachosuchus* demonstrate similar patterns of biting-induced stress to that of the gharial?

(2) Does the premaxillary palate of *Ebrachosuchus* confer the same structural advantages as the secondary palate of extant crocodilians, namely does it provide additional resistance to bending and torsion?

(3) Does the retention of the antorbital fenestra result in lower resistance to bending, torsion and biting-induced stress in the skull of *Ebrachosuchus* compared to the gharial?

Skull Reconstruction

The skull of *Ebrachosuchus* had to be digitally reconstructed (Fig. 3). *Ebrachosuchus* showed the most damage along the premaxillary palate: the premaxillary shelves (which extend laterally and meet along the midline of the skull to form the premaxillary palate) were broken and displaced. Segments of the shelves were manually realigned while the most damaged region, encompassing the ventral surface of the mid-anterior to anterior regions of the rostrum, were completely removed and manually rebuilt. Damage to the alveolar cavities was predominately confined to the left half of the rostrum thus the right half was mirrored to compensate for the damage. Similarly, the left half of the terminal rosette was mirrored to replace the right half of the terminal rosette, which was deformed and lacked clear differentiations of the alveolar cavities. The left lateral rim of the external nares were damaged and replaced by a mirrored section of the right lateral rim. The rim of the left antorbital fenestra and adjacent section of the maxilla was deformed and displaced; this section was replaced by a mirrored section of the right maxilla. The palatines showed some damage and, because they are thin bone, were not isolated automatically and had to be reformed manually. Along the midline of the pterygoids we expect to see thin shelves extending laterally from the pterygoids to the palatines forming a closed palate region as in other phytosaurs (Dzik, 2001); however, these are not preserved in *Ebrachosuchus* and were manually recreated along with additional reconstruction of the pterygoids and vomers.

142 **Beam Theory**

143 Beam theory calculations were carried out using ImageJ (http://rsbweb.nih.gov/ij) with the
144 MomentMacro plugin (http://www.hopkinsmedicine.org/fae/mmacro.htm). A total of 20 CT
145 slices were taken from *Ebrachosuchus*, the gharial, the alligator and the slender-snouted crocodile
146 (Fig. 4). Four transverse slices were taken through the terminal rosette of each specimen and the
147 remaining 16 transverse slices were taken at evenly spaced intervals along the skull, extending as
148 far as the posterior extent of the tooth row (Fig. 4). Three measurements were recorded: Ix, the
149 second moment of area about the mediolateral axis of the snout and a proxy for resistance to
150 dorsoventral bending; Iy, the second moment of area about the dorsoventral axis of the snout and
151 a proxy for resistance to mediolateral bending; J, the polar moment of inertia and the sum of Ix
152 and Iy, a proxy for resistance to torsion. These values were standardized for size in order to
153 accurately compare patterns of resistances between taxa. This standardization was done by
154 calculating the resistance to bending and torsion of a circle with equal cortical area for each slice.
155 The absolute resistances for each
156 slice of the skull were then divided by the corresponding circle resistances. This provides an
157 estimate of how far snout shape deviates from a circle rather than a magnitude of bending and
158 torsion resistance. To assess the functional implications of the premaxillary palate in
159 *Ebrachosuchus*, resistances to bending and torsion were calculated both with the palate and with
160 the palate removed, and were then compared to the extant taxa both with and without their
161 secondary palates. The secondary palates were manually removed in each CT slice using ImageJ.
162 The secondary palates were easily differentiated in the CT slices as the ventral surface of the
163 rostrum lying between the dental alveoli.

164 **Surface Construction**

CT scans were used to generate 3D digital skull models that were discretized into finite element models (FEMs) for *Ebrachosuchus*, the alligator, the gharial, and the Nile crocodile. The skull of *Ebrachosuchus* was scanned at the Klinikum rechts der Isar, Munich. Scans of the American alligator (*Alligator mississippiensis*: TMM m-983, sub-adult, skull length 217 mm) were obtained from 'Digital Atlas of the Alligator' (Rowe et al. 1999); *Gavialis gangeticus* scans were acquired at the Royal Veterinary College from a large gharial specimen (NHMUK 2005.1605, approximately 80 cm skull length); scans of *Crocodylus niloticus* were also obtained at the Royal Veterinary College (specimen RVC AN1, 501 mm total skull length), donated by the La Ferme aux Crocodiles conservation park. CT scans were also obtained of the slender-snouted crocodile *Mecistops cataphractus* (NHMUK 1924.5.10.1, adult with skull length 62 cm), also scanned at the Royal Veterinary College.

CT scans were assessed in Avizo (VSG, Massachusetts) where a label field was generated to isolate the bone from surrounding tissue or matrix. Each slice was manually edited to ensure all desired components of the skull were selected and to remove and fill in holes in the surface. The teeth of four skulls were removed and the alveolar cavities were filled in in order to reconcile the crocodilian models to *Ebrachosuchus*, in which the dentition is largely unpreserved. In order to test the effects of the antorbital fenestra on stress in *Ebrachosuchus*, an additional model was made of *Ebrachosuchus* in which the antorbital fenestra is filled in.

FEMs of all specimens without the palates were created in Avizo by adjusting the label field of each CT slice and removing the bony material of the palate, similar to the method described above in creation of the beam theory models.

Finite element models

Surfaces were imported into Hypermesh (Altair, Michigan) as FEMs composed of 2D elements. These models were inspected and imperfections, such as distorted elements and

element intersections, were corrected before the models were re-meshed with 3D elements. Completed 3D models were then imported into Abaqus (3DS, France) for FEA. Convergence tests were used to determine the size of the elements, and the resolution of the mesh, necessary for the model to solve completely; at this point, any increase in the resolution of the mesh has no effect on the results of the FEA.

Convergence testing (Bright & Rayfield, 2011) was carried out to assess the optimum mesh size for *Ebrachosuchus*. Four models were generated for the convergence test: Model 1 at 250,000 elements, Model 2 at 600,000 elements, Model 3 at 3 million elements, and Model 4 at 5 million elements. Models 1–4 were created with four-noded linear elements (TET4) while two addition versions of Models 3 and 4 were created with 10-noded quadratic elements (TET10) for comprehensive comparisons. TET10 typically improve results compared to TET4 models (Owen & Saigal, 2001) by having more nodes per element; however, these TET10 models showed minimal difference to their respective TET4 models as well as a significant increase in computation time. Optimal mesh sizes for the crocodilian taxa were then approximated based on previous studies involving FEA utilizing the same specimens (Rayfield et al., 2007; Adams, 2011).

Boundary conditions

The four skull models were assigned uniform material properties, boundary conditions and loading regimes. Following most previous FEA studies of extinct taxa, all models were assigned elastic isotropic properties with the following values: Young's modulus (E) = 10 GPa; Poisson's ratio (ν) = 0.4 (values after Rayfield et al. 2001).

Models were constrained at the articulation of the quadrate with the lower jaw and on the basiocciput; chosen nodes were constrained against three translational degrees of freedom. Stiffness of the skulls was tested through ten loading conditions on each skull: five bilateral loads

consisting of two symmetrical 500 N forces (one on each tooth row) and five unilateral loads consisting of one 1000 N force on the working tooth row (Fig. 5). These loads were placed on the ventral surface of the skull at one of five different locations along the tooth row, and directed dorsally. Additional loads perpendicular to the dorsally directed loads were included to model the lateral flexion of the skull during "head shaking" proposed by McHenry et al., (2006; Fig. 5); a dorsal and laterally directed pair of 500 N loads.

In order to remove the effect of size from the analysis and test for the capability of different skull shapes to withstand feeding loads, all applied loads were scaled to the same force per unit surface area of the skull (Dumont, Grosse & Slater, 2009). Force values quoted above are the original values applied to *Ebrachosuchus*, to which all other models were scaled.

Analysis

Von Mises stress (a combination of the three principal stresses) has shown to correlate with ductile failure while brittle failure has been correlated with maximum principal stress (Juvinall & Marshek, 2006); due to their material properties, these skulls would likely fail under a ductile mode of fracture and thus von Mises stress is used as an indicator of relative cranial strength (Nalla, Kinney & Ritchie, 2003; Dumont, Grosse & Slater, 2009). Von Mises values were taken along dorsal midline of the rostra at five positions corresponding to the location of the five loading conditions: anterior tip, mid anterior, mid, mid posterior, and posterior.

Maximum principal stress shows areas of the skull under tension. As bone is weaker in tension than compression (Currey, 2002), maximum principal stress was used as an indicator of how the skulls respond to biting loads and the influence on mechanical behaviour of the structural differences between crocodilian and phytosaur skulls. Maximum principal stress values were taken along the ventral surface of the skull at the same five midline positions as before. The ventral surface was chosen as this region experiences high tensile stress values during loading.

Maximum principal values for models without the palate were taken along the tooth row as the ventral surface had been removed and the resultant tensions were concentrated along the tooth rows; i.e., maximum stress values along the venter of the rostrum were compared between models.

The final variable of interest was strain energy. Strain energy is the energy stored in a structure due to deformation. The minimization of strain energy in the skull is interpreted as beneficial for the organism by maximizing work efficiency and transfer of load without deflection of the skeleton. Strain energy is associated with failure through deflection (Dumont, Grosse & Slater, 2009). A rostrum that does not maintain rigidity and instead bends when the animal bites down on a prey item makes prey capture exceptionally difficult. In order to accurately compare strain energy between models, the strain energy values are scaled to the same force per unit volume (Dumont, Grosse & Slater, 2009).

Results

Beam Theory

Ebrachosuchus, the alligator, the gharial, and the slender-snouted African crocodile all show relatively stable resistance to dorsoventral bending passing from anterior to posterior along the rostrum with a dramatic increase in the final five slices (Fig. 6). Within these taxa, *Ebrachosuchus* shows marginally higher resistance to mediolateral bending and torsion (Fig. 6) than the gharial (which shows the lowest resistance to these forces) and slender-snouted African crocodile, but all three show much lower resistance to mediolateral bending and torsion than the alligator.

The removal of the palate results in a slight but persistent reduction in resistance to dorsoventral bending in both *Ebrachosuchus* and the gharial (Fig. 7). Resistance to mediolateral bending and torsion are minimally affected by the removal of the premaxillary/secondary palate.

Finite Element Analysis

Comparative analyses between all taxa show *Ebrachosuchus* to have the lowest structural resistance under all loading conditions (Fig. 8 and 9). Rostral von Mises stress values in *Ebrachosuchus* range from eight times greater compared to the equivalent loading positions in the gharial, to over 100 times greater compared to the Nile crocodile (Table S1). *Ebrachosuchus* shows the highest stresses around the mid-anterior to mid regions while the gharial shows the highest stresses in the mid to mid-posterior region (Fig. 10) while both the alligator and the Nile crocodile show the highest stress values in the post-orbital region of the skull. Removal of the secondary palate in the gharial and the premaxillary palate of *Ebrachosuchus* results in a general increase in the maximum observed von Mises stress magnitudes for both taxa (Fig. 8). Peak von Mises stress for *Ebrachosuchus* shifts posteriorly towards the nares while the gharial shows only a proportional increase in observed stress with no shift in the peak stress position along the rostrum (Fig. 8B and Fig. 9B). Removing the antorbital fenestra in *Ebrachosuchus* generally decreased the observed von Mises values in all loading conditions and increased structural resistance.

Maximum principal stress exhibits similar patterns as von Mises stress across all four taxa (Fig. 8). *Ebrachosuchus* shows the highest levels of stress (especially in the mid-rostral regions) compared to any of the extant crocodilians. Head shaking loads show roughly half the peak maximum principal stress (and von Mises stress) compared to the bilateral loading conditions at the equivalent loading positions for all taxa (Table S2). Removal of the palates of *Ebrachosuchus* and the gharial elevate the maximum principal stress in the mid-posterior and

posterior regions (Fig. 9, 11). According to the queried nodes, the peak maximum principal stress is elevated in the gharial by the removal of the palate; conversely, the peak tension is decreased in *Ebrachosuchus* with the removal of the palate; however, observing the finite element model as a whole shows an increase in peak von Mises on the dorsal and ventral surfaces and an increase in the expanse of the high stress contours (Fig. 11). Removal of the antorbital fenestra of *Ebrachosuchus* decreases the peak tension, though not as much as removal of the palate, but maintains the overall pattern seen in the original morphology.

Ebrachosuchus possessed the highest strain energy (Table S3) for bilateral, unilateral, and head-shaking loads. The trend among the crocodilians was also consistent across all three loading regimes: the alligator showed the greatest minimization of strain energy followed closely by the Nile crocodile, with the gharial showing the highest strain energy of the three extant taxa (Fig. 12A). Removal of the palate in *Ebrachosuchus* and the gharial increased the calculated strain energy for both taxa (Fig. 12B): in the gharial the increase was up to 18% (under unilateral loading conditions) with the palate removed, whereas in *Ebrachosuchus* the increase was up to 14% (under head-shaking loading conditions). *Ebrachosuchus*, under all loading conditions, and both with and without the premaxillary palate and antorbital fenestra, retained much higher strain energy than any of the crocodilians (Fig. 12).

Discussion

Structural Convergence

Beam theory and FEA show that *Ebrachosuchus* responds similarly to slender-snouted extant crocodilians (i.e. the gharial and the slender-snouted crocodile) in terms of resistance to mediolateral bending, torsion and patterns of accommodation of stress. The Nile crocodile and

the alligator show the greatest degree of platyrostry, and this produces a higher resistance to mediolateral bending and torsion as demonstrated in the alligator by beam theory. The Nile crocodile shows both the greatest surface area of any specimen used in the FEA and the lowest force per unit area, corresponding to the most efficient accommodation of stress; this observation is perhaps unsurprising given that the Nile crocodile is a large-bodied apex predator.

The gharial behaves more like *Ebrachosuchus* in the accommodation of von Mises and maximum principal stress than do either the alligator or the Nile crocodile. However, *Ebrachosuchus* shows higher levels of stress and much greater strain energy than in any of the extant taxa. These observations suggest that the skull of *Ebrachosuchus* was more susceptible to failure than those of the extant taxa under equivalent loading conditions. Removal (in-filling) of the antorbital fenestra decreased the queried stress values on the rostrum; however, its removal also increased the total strain energy. It must be noted that the queried nodes, due to position and/or relatively small number reflect local values that may not be indicative of overall trends as shown in Figures 10 and 11.

Phytosaurian Palate

We provide the first quantitative support for the hypothesis that at least one key function of the phytosaurian premaxillary palate, which ventrally bounded an extensive paranasal sinus, is to assist the skull in the dispersal of stress (Witmer, 1997). We therefore consider the premaxillary palate as analogous, in functional terms, to the secondary palate of crocodilians. The crocodilian secondary palate separates the nasal and buccal cavities and permits breathing and feeding while submerged (Cleuren & De Vree, 2000), but it also imparts important resistances to stress during feeding (Thomason & Russell, 1986; Busbey, 1995; McHenry et al., 2006; Rayfield et al., 2007; Walmsley et al., 2013). Beam theory and FEA show that the removal of the premaxillary palate of *Ebrachosuchus* causes a decrease in resistance to dorsoventral bending and

329 increases the observed von Mises values and maximum principal stress in the elongated rostrum.
330 As phytosaurs do not utilise the premaxillary palate for respiratory purposes, our work provides
331 independent support that the premaxillary palate functioned to resist feeding-induced stress. The
332 independent acquisition of a true secondary palate combined with the loss of the antorbital
333 fenestra in crocodilians provided increased resistance to stress and better work efficiency
334 compared to *Ebrachosuchus*, and potentially phytosaurs in general.

335 **Feeding ecology**

336 The gharial and the alligator represent the most divergent forms of crocodilian
337 morphology, with the slender-snouted crocodile lying between the two (Pierce, Angielczyk &
338 Rayfield, 2008). Based on its structural similarity to the gharial, we support previous
339 interpretations of the extreme longirostrine rostrum of *Ebrachosuchus* as a morphological
340 response to an aquatic ecology and a diet dominated by small fish. Our functional results suggest
341 that the longirostrine morphology of this taxon is unlikely to have been able to accommodate the
342 stress of subduing relatively large prey, thus differing from the feeding habits of large alligators
343 and the Nile crocodile. This interpretation is based upon the dispersion of stress across the
344 rostrum of the alligator and Nile crocodile, whereas stress is concentrated along the rostrum of
345 *Ebrachosuchus* and the gharial.

346 The only possible direct evidence for diet in longirostrine phytosaurs comes from stomach
347 contents: two specimens of the longirostrine basal phytosaur *Parasuchus* (phylogenetically close
348 to *Ebrachosuchus*) were reportedly found each with a small archosauromorph reptile skeleton and
349 one with a few skull bones of a rhynchosaur in the area of the stomach cavity (Chatterjee, 1978).
350 However, no taphonomic analysis of this specimen (necessary to demonstrate that all of the
351 preserved remains do in fact represent stomach contents) has been published. Chatterjee (1978)
352 suggested that, in the case of small prey, the prey item would be swallowed completely. By

353 contrast, if the prey item were too large to swallow (as in the case of the rhynchosaur), it would
354 be mechanically reduced to smaller, manageable pieces. Assuming that the morphologically
355 similar *Parasuchus* exhibited similar patterns of stress to those recovered here for
356 *Ebrachosuchus*, it is questionable that this species would have been capable of mechanically
357 breaking the robust skull of a rhynchosaur. Thus, the fragments of a rhynchosaur skull found with
358 *Parasuchus* may already have been disarticulated prior to ingestion, or may prove not to be
359 stomach contents.
360

361 ## Conclusions

362 1. *Ebrachosuchus* and the gharial both show similar patterns of stress under feeding
363 related loading conditions, with high stress forming along the rostrum. However,
364 *Ebrachosuchus* shows much higher stress and strain energy under these loading
365 conditions compared to any crocodilian.
366 2. Removal of the premaxillary palate in *Ebrachosuchus* and the secondary palate of
367 crocodilians shows that both contribute to strengthening the skull in its resistance to
368 stress and bending.
369 3. Removal of the antorbital fenestra in *Ebrachosuchus* decreases the magnitude of stress
370 developed from our load conditions indicating the antorbital fenestra does indeed
371 slightly weaken the skull.

372 Our results provide further evidence for independent evolution of functionally convergent
373 longirostrine morphotypes across vertebrate evolutionary history. However, in the case of
374 phytosaurs, the secondary palate-like structure formed by the premaxillae apparently serves the
375 purpose of conferring structural strength to the skull, without the benefit (present in true

secondary palates) of separating the nasal and oral chambers to facilitate breathing and respiration. Our analyses provide further evidence of the structural compromises induced by a key archosauriform feature, the antorbital fenestra.

Acknowledgements

We thank Martin Dobritz (Klinikum rechts der Isar, Munich) for CT scanning of *Ebrachosuchus* and Oliver Rauhut (BSPG, Munich) for access to specimens; Chris Lamb (Royal Veterinary College, London) for CT scanning extant crocodilian specimens.

References

Adams W. 2011. Ontogeny of *Crocodylus niloticus* cranial mechanics. Bristol: University of Bristol.

Bright JA., Rayfield EJ. 2011. The response of cranial biomechanical finite element models to variations in mesh density. *Anatomical Record* 294:610–620. DOI: 10.1002/ar.21358.Brochu C. 2012. Phylogenetic relationships of Palaeogene ziphodont eusuchians and the status of *Pristichampsus* Gervais, 1853. *Earth and Environmental Science Transactions of the Royal Society of Edinburgh* 103:521-550. DOI: 10.1017/S1755691013000200

Bronzati M., Montefeltro FC., Langer MC. 2012. A species-level supertree of Crocodyliformes. *Historical Biology* 24:598-606. DOI: 10.1080/08912963.2012.662680

Brusatte SL., Butler RJ., Niedzwiedzki G., Sulej T., Satkunas J. 2013. First record of Mesozoic terrestrial vertebrates from Lithuania: phytosaurs (Diapsida: Archosauriformes) of probable Late Triassic age, with a review of phytosaur biogeography. *Geological Magazine* 150:110–122.

399 Busbey AB. 1995. The structural consequences of skull flattening in crocodilians. In: Thomason
400 JJ ed. *Functional morphology in vertebrate paleontology*. Cambridge: Cambridge
401 University Press, 173–192.
402 Butler RJ., Rauhut OWM., Stocker MR., Bronowicz R. 2014. Redescription of the phytosaurs
403 *Paleorhinus* ('*Francosuchus*') *augustifrons* and *Ebrachosuchus neukami* from Germany,
404 with implications for Late Triassic biochronology. *Zoological Journal of the Linnean*
405 *Society* 170:155–208.
406 Camp CL. 1930. A study of phytosaurs with descriptions of new material from western North
407 America. *Memoirs of the University of California* 10:1–174.
408 Chatterjee S. 1978. A primitive parasuchid (phytosaur) reptile from the Upper Triassic Maleri
409 Formation of India. *Palaeontology* 21:83–127.
410 Cleuren J., De Vree F. 2000. Feeding in crocodilians. In: Schwenk K ed. *Feeding: Form,*
411 *Function, and Evolution in Tetrapod Vertebrates*. San Diego: Academic Press, 337–358.
412 Colbert EH. 1947. Studies of the phytosaurs *Machaeroprosopus* and *Rutiodon*. *Bulletin of the*
413 *American Museum of Natural History* 88:53–96.
414 Currey JD. 2002. *Bones: Structure and Mechanics*. Princeton, N.J.: Princeton University Press.
415 Daniel WJT., McHenry CR. 2001. Bite force to skull stress correlation - modelling the skull of
416 *Alligator mississippiensis*. In: Grigg GC, Seebacher F, Franklin CE eds. *Crocodilian*
417 *Biology and Evolution*. NSW, Australia: Surrey Beatty & Sons, 135–143.
418 Dumont ER., Grosse IR., Slater GJ. 2009. Requirements for comparing the performance of finite
419 element models of biological structures. *Journal of Theoretical Biology* 256:96–103. DOI:
420 10.1016/j.jtbi.2008.08.017.
421 Dzik, J. 2001. A new *Paleorhinus* fauna in the Early Late Triassic of Poland. *Journal of*
422 *Vertebrate Paleontology* 21:625-627.

423 Ennos AR. 2012. *Solid Biomechanics*. Princetone, N.J.: Princeton University Press.

424 Ezcurra MD. 2016. The phylogenetic relationships of basal archosauromorphs, with an emphasis
425 on the systematics of proterosuchian archosauriforms. *PeerJ* 4:e1778.
426 https://doi.org/10.7717/peerj.1778

427 Gregory JT. 1962. The genera of phytosaurs. *American Journal of Science* 260:652–690. DOI:
428 10.2475/ajs.260.9.652.

429 Hungerbühler A. 2000. Heterodonty in the European phytosaur *Nicrosaurus kapffi* and its
430 implications for the taxonomic utility and functional morphology of phytosaur dentitions.
431 *Journal of Vertebrate Paleontology* 20:31–48.

432 Hunt AP. 1989. Cranial morphology and ecology among phytosaurs. In: Lucas SG, Hunt AP eds.
433 *Dawn of the Age of Dinosaurs in the American Southwest*. Albuquerque: New Mexico
434 Museum of Natural History, 349–354.

435 Hunt A., Lucas S. 1991. The *Paleorhinus* biochron and the correlation of the nonmarine Upper
436 Triassic of Pangea. *Palaeontology* 34:487–501.

437 Jones AS, Butler RJ. 2018. A new phylogenetic analysis of Phytosauria (Archosauria:
438 Pseudosuchia) with the application of continuous and geometric morphometric character
439 coding. *PeerJ* 6:e5901. DOI: 10.7717/peerJ.5901.

440 Juvinall RC., Marshek KM. 2006. *Fundamentals of Machine Component Design*. New York:
441 Wiley.

442 Kimmig J., Arp G. 2010. Phytosaur remains from the Norian Arnstadt Formation (Leine Valley,
443 Germany) with reference to European phytosaur habits. *Palaeodiversity* 3:215–224.

444 Lautenschlager S., Butler RJ. 2016. Neural and endocranial anatomy of Triassic phytosaurian
445 reptiles and convergence with fossil and modern crocodylians. *PeerJ* 4:e2251. DOI:
446 10.7717/peerj.2251.
447 McGregor JH. 1906. The Phytosauria, with especial reference to *Mystriosuchus* and *Rhytiodon*.
448 *Memoirs of the American Museum of Natural History* 9:30–101.
449 McHenry CR., Clausen PD., Daniel WJT., Meers MB., Pendharkar A. 2006. Biomechanics of the
450 rostrum in crocodilians: a comparative analysis using finite-element modeling. *The*
451 *Anatomical Record. Part A, Discoveries in Molecular, Cellular, and Evolutionary Biology*
452 288:827–849. DOI: 10.1002/ar.a.20360.
453 Nalla RK., Kinney JH., Ritchie RO. 2003. Mechanistic fracture criteria for the failure of human
454 cortical bone. *Nature Materials* 2:164–168. DOI: 10.1038/nmat832.
455 Nesbitt SJ. 2011. The early evolution of archosaurs : relationships and the origin of major clades.
456 *Bulletin of the American Museum of Natural History* 352:1–292.
457 Owen SJ., Saigal S. 2001. Formation of pyramid elements for hexahedra to tetrahedra transitions.
458 *Computer Methods in Applied Mechanics and Engineering* 190:4505–4518. DOI:
459 10.1016/S0045-7825(00)00330-3.
460 Pierce SE., Angielczyk KD., Rayfield EJ. 2008. Patterns of morphospace occupation and
461 mechanical performance in extant crocodilian skulls: a combined geometric morphometric
462 and finite element modeling approach. *Journal of Morphology* 269:840–864. DOI:
463 10.1002/jmor.10627.
464 Rayfield EJ., Milner AC., Xuan VB., Young PG. 2007. Functional morphology of spinosaur
465 “crocodile-mimic” dinosaurs. *Journal of Vertebrate Paleontology* 27:892–901.
466 Rayfield EJ., Norman DB., Horner CC., Horner JR., Smith PM., Thomason JJ., Upchurch P.
467 2001. Cranial design and function in a large theropod dinosaur. *Nature* 409:1033–1037.

Stocker MR., Butler RJ. 2013. Phytosauria. *Geological Society, London, Special Publications* 379:SP379.5. DOI: 10.1144/SP379.5.

Thomason JJ., Russell AP. 1986. Mechanical factors in the evolution of the mammalian secondary palate: a theoretical analysis. *Journal of Morphology* 189:199–213. DOI: 10.1002/jmor.1051890210.

Walmsley CW., McCurry MR., Clausen PD., McHenry CR. 2013. Beware the black box: investigating the sensitivity of FEA simulations to modelling factors in comparative biomechanics. *PeerJ* 1:e204. DOI: 10.7717/peerj.204.

Witmer LM. 1997. The evolution of the antorbital cavity of archosaurs: a study in soft-tissue reconstruction in the fossil record with an analysis of the function of pneumaticity. *Journal of Vertebrate Paleontology* 17:1–76. DOI: 10.1080/02724634.1997.10011027.

480 **Table 1.** Specimen Details

Taxon	Specimen ID.	Number of Slices	Slice Spacing (mm)	Analyses
Ebrachosuchus neukami	BSPG 1931X 501	1634	0.6	Beam Theory, FEA
Gavialis gangeticus	BMNH 2005.1605	161	5	Beam Theory, FEA
Alligator mississippiensis	TMM M-983	135	0.48	Beam Theory, FEA
Crocodylus niloticus	RVC AN1	210	3	FEA
Crocodylus cataphractus	BMNH 1924.5.10.1	128	5	Beam Theory

481

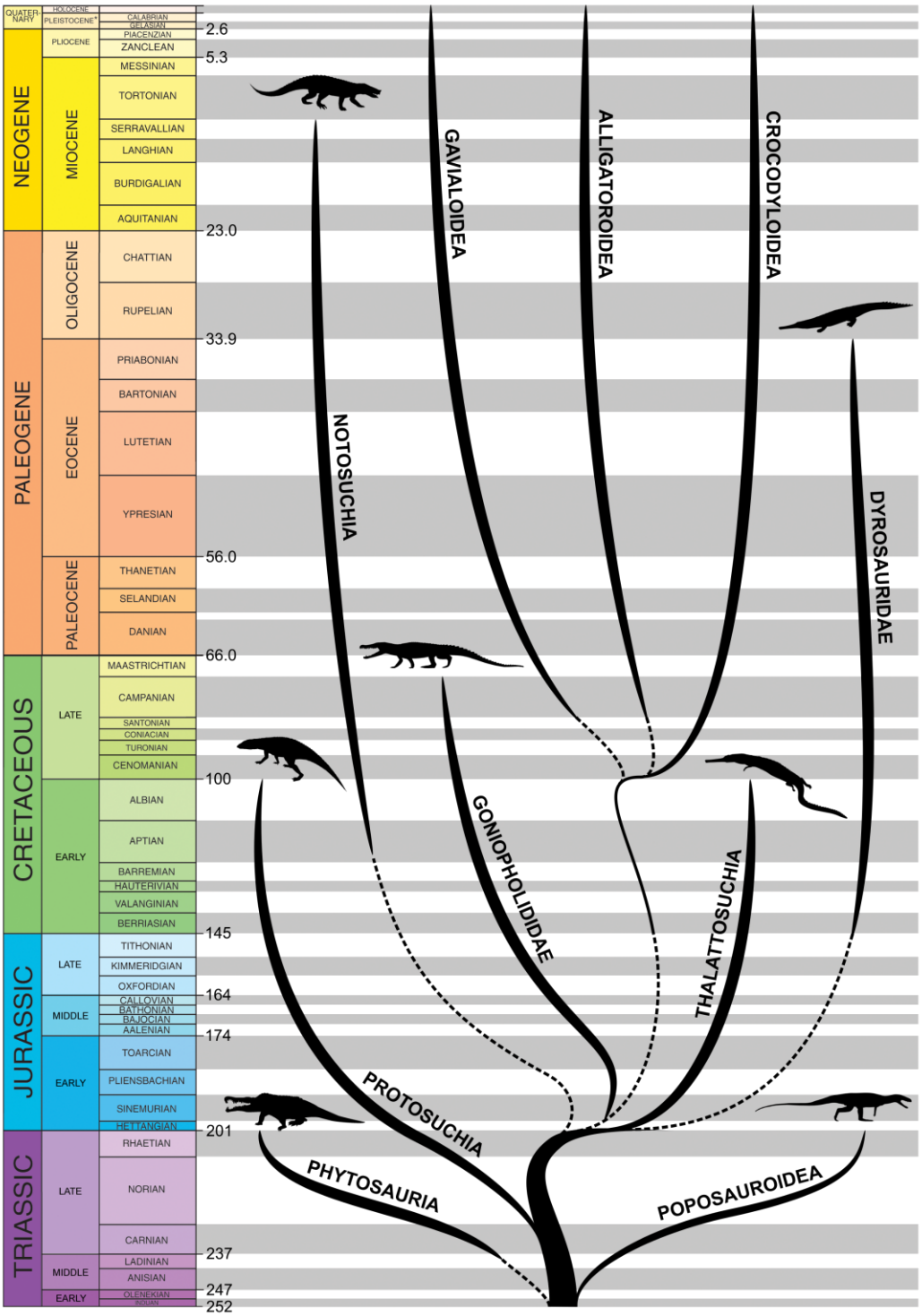

Figure 1.**Simplified phylogeny of Pseudosuchia.** Simplified time-calibrated phylogeny showing the relationships within Pseudosuchia, the clade that includes modern crocodilians and their stem-lineage, including phytosaurs. This phylogeny is based on data from Nesbitt (2011), Bronzati et al. (2012), Brochu (2012), and Ezcurra (2016) with stratigraphic ranges drawn primarily from the Paleobiology Database (www.paleobiodb.org). Note that c. 100 million years separates the extinction of phytosaurs and the origins of crown group crocodilians (Gavialoidea + Alligatoroidea + Crocodyloidea).

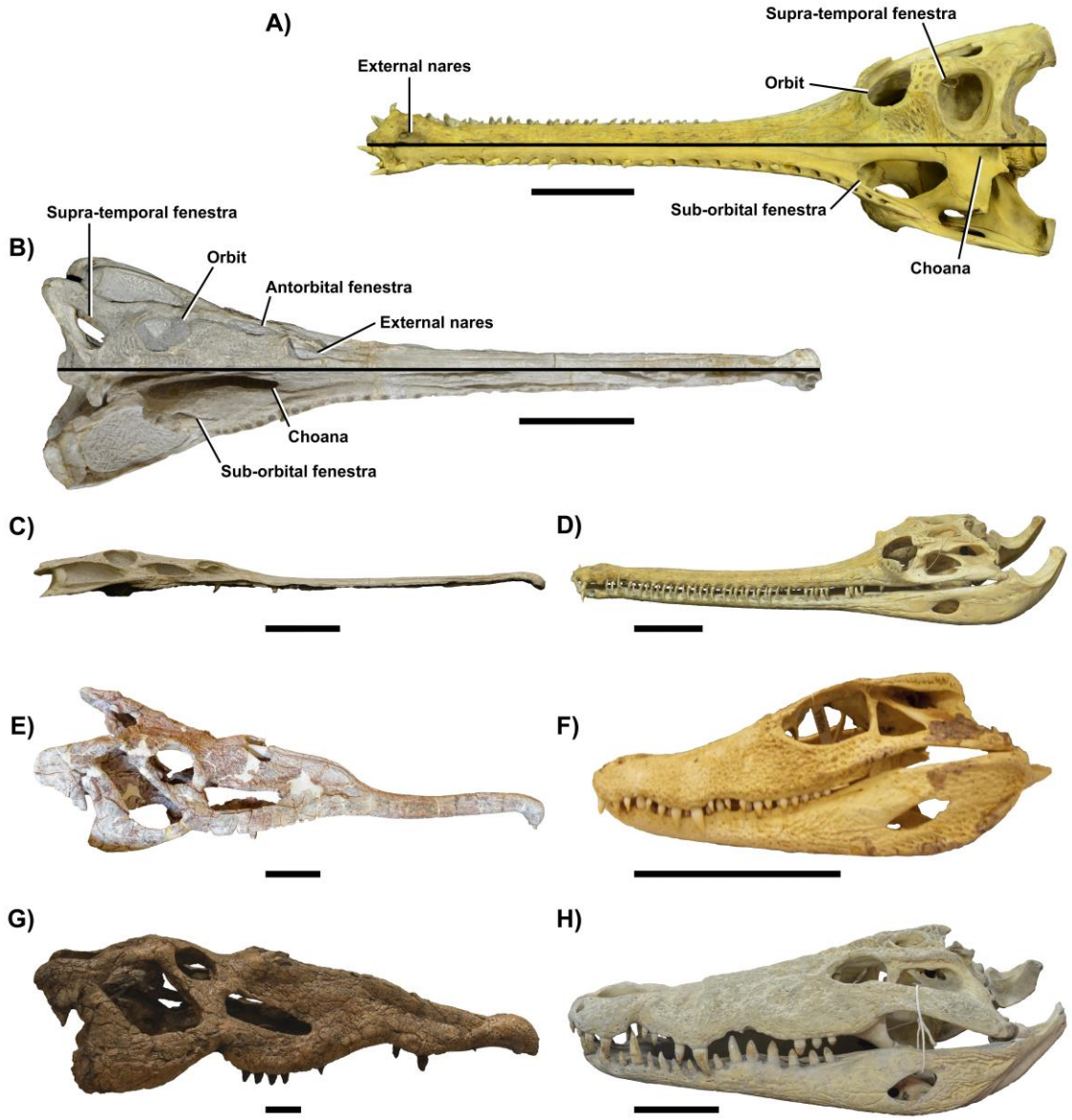

Figure 2.Comparative cranial anatomy between crocodilians and phytosaurs. Comparison between the cranial morphology of (a) the gharial and (b) *Ebrachosuchus*, with the upper and lower halves of each skull displaying dorsal and ventral morphologies respectively. Furthermore, representatives of both (c, e, g) phytosaurs and (d, f, h) crocodilians demonstrating the three ecomorphotypes proposed by Hunt (1989): (c, d) *Ebrachosuchus neukami* (BSPG 1931 X 501) and *Gavialis gangeticus* (BMNH 1935.6.4.1) exhibiting the slender-snouted form, (e, f) *Leptosuchus* spp. (TMM 31173-120) and *Paleosuchus palpebrosus* (AMNH R-58136) representing the moderate-snouted form, and (g, h) *Smilosuchus gregorii* (AMNH FR-3060) and *Crocodylus niloticus* (BMNH 1959.1.8.55) exemplifying the massively-snouted form. Scale bars = 100mm.

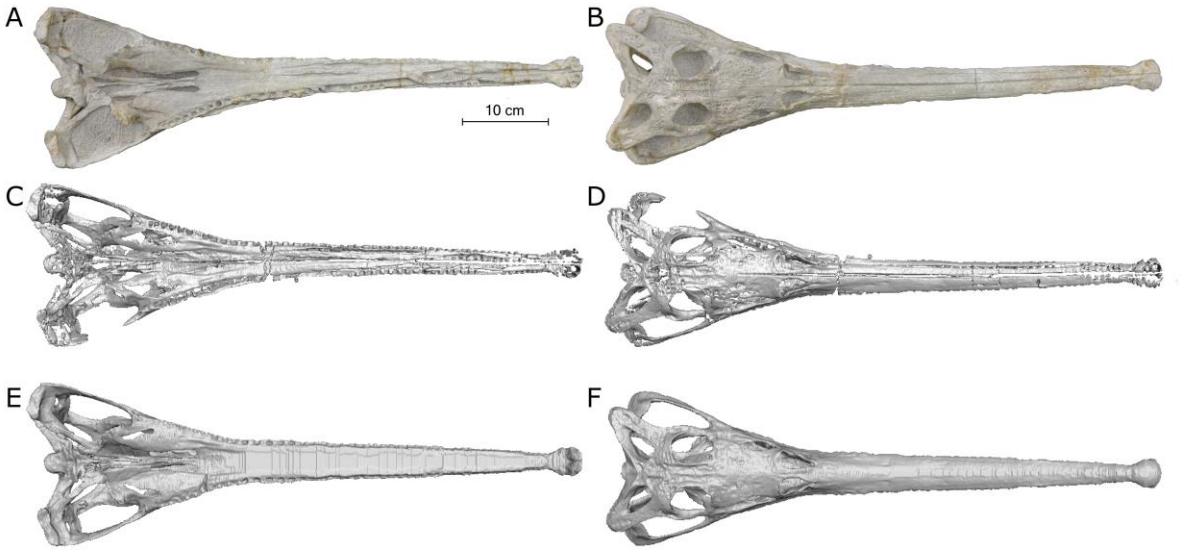

Figure 3. **Reconstruction of the skull of *Ebrachosuchus*.** Comparison of the ventral (A,C,E) and dorsal (B,D,F) views of the original skull of *Ebrachosuchus neukami* (A,B), segmented bone data (C,D), and final reconstructed model (E,F).

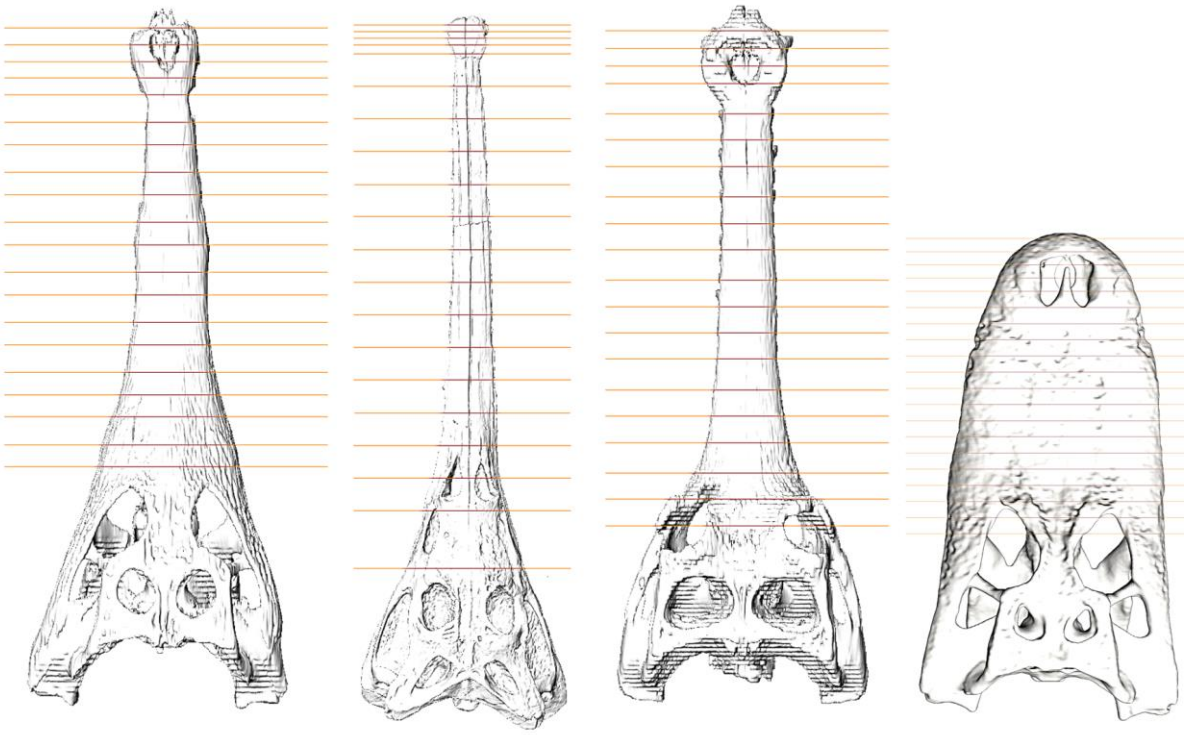

Figure 4. Beam theory slice locations. Location of the slices taken for beam theory analysis. From left to right: slender-snouted crocodile, *Ebrachosuchus*, the gharial, and the American alligator.

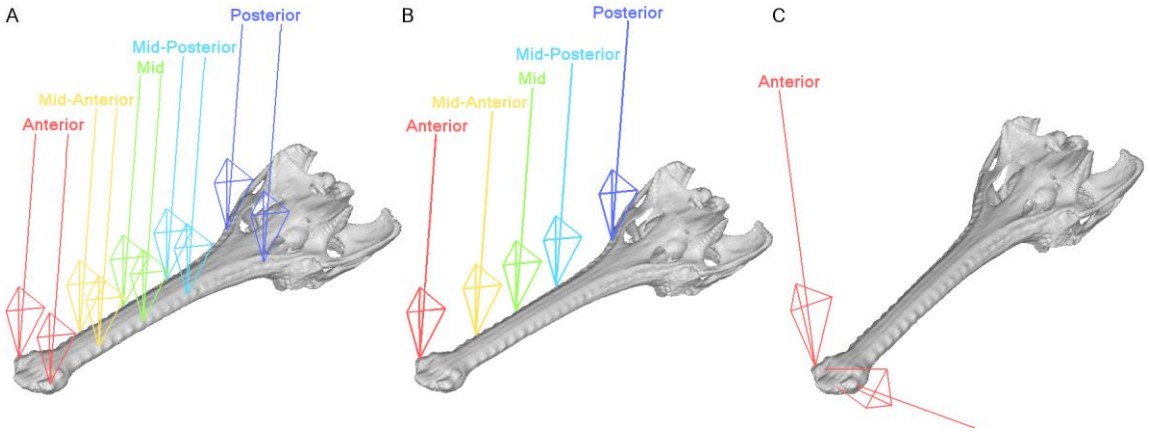

506

507 **Figure 5**. **Orientations and locations of load cases.** The loading conditions used for the finite element
508 analysis shown on the skull of the Gharial. Each set of colored arrows represents and independent loading
509 case. (A) Bilateral load cases, each pair of 500N loads is run as a separate analysis. (B) The five 1000 N
510 unilateral load cases. Each loading case is named after its location on the skull; starting from the anterior
511 most load(s): Anterior, Mid-Anterior, Mid, Mid-Posterior, Posterior. (C) Example of the anterior head-
512 shaking loading condition. Head-shaking cases were also done for each of the five locations along the
513 tooth row.

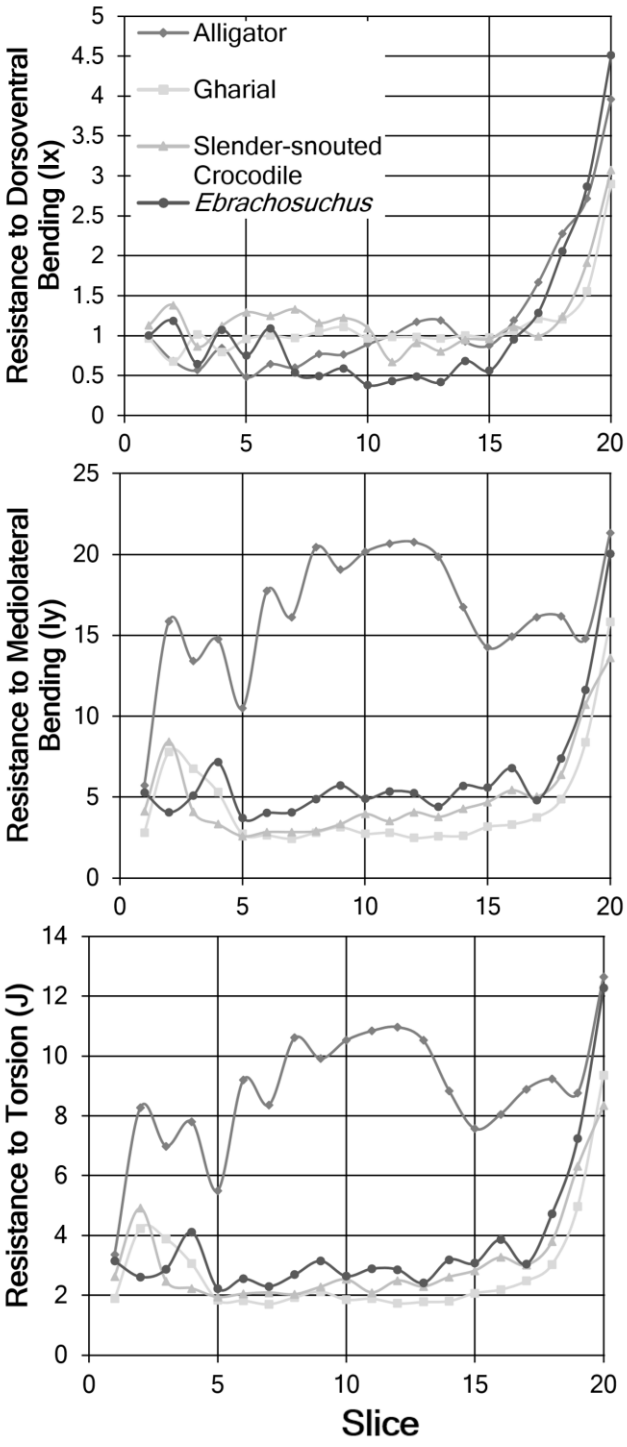

514

515 **Figure 6**. **Beam theory results from the original skull morphologies.** Results of the beam theory
516 analysis for the alligator, the gharial, the slender-snouted crocodile, and the basal phytosaur
517 *Ebrachosuchus*. All specimens show increasing resistance to dorsoventral bending going from anterior to
518 posterior. The alligator shows the greatest resistance to mediolateral bending, likely due to the extremely
519 flat and broad snout shape relative to the other specimens, this also leads to a high resistance to torsion for
520 the entire rostrum. Slice number begins at the anterior most slice (slice 1) and extends posteriorly until the
521 posterior most slice (slice 20).

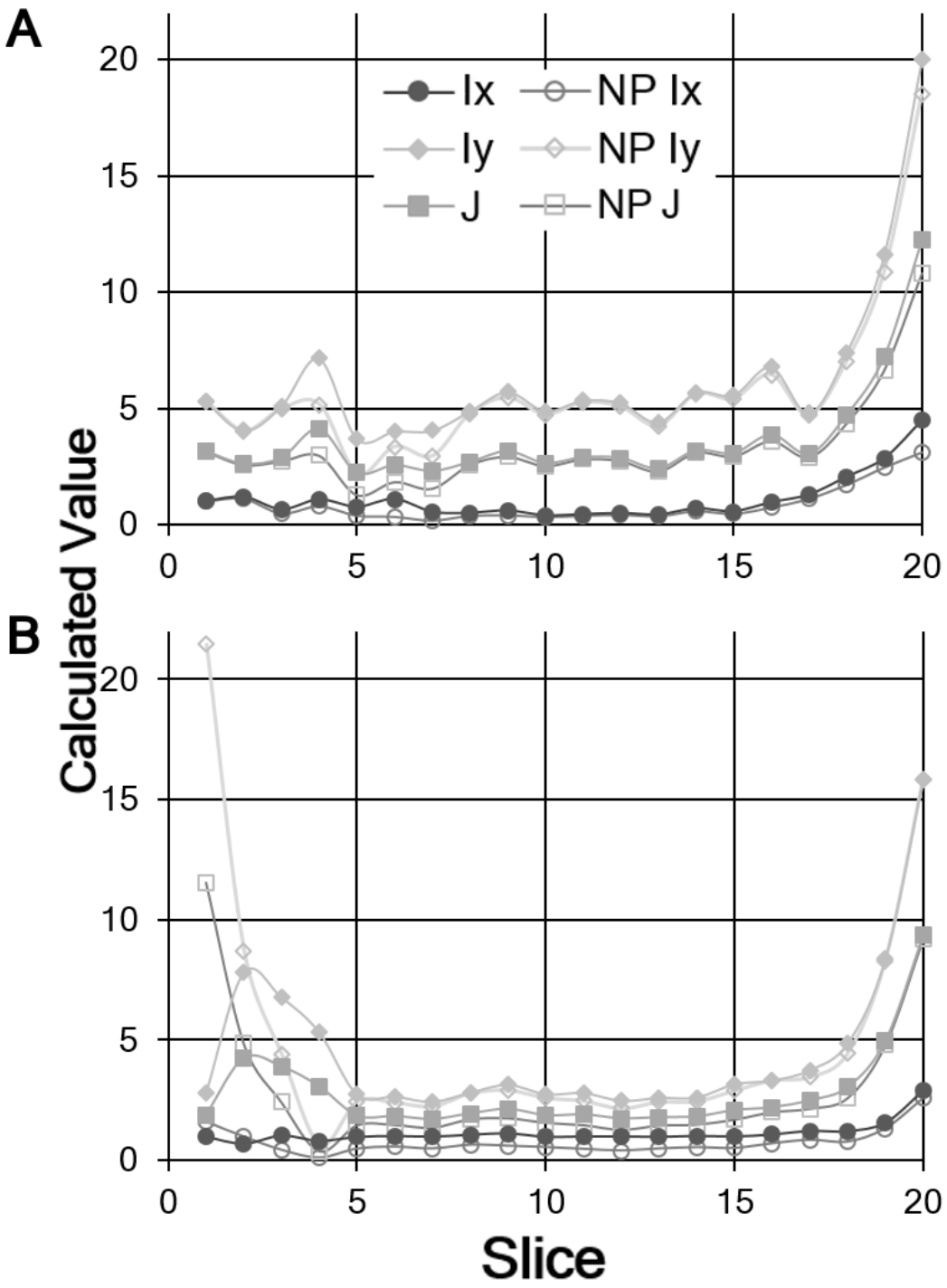

Figure 7. **Beam theory results from the theoretical skull morphologies.** Comparison of the beam theory analysis for (a) *Ebrachosuchus* and (b) the gharial for both regular models and models with the palates removed (NP). Ix is resistance to dorsoventral bending, Iy is the resistance to mediolateral bending, and J is the resistance to torsion. In general, removing the palate causes a very slight decrease in resistance to bending with a notable exception be the first two slices of the gharial.

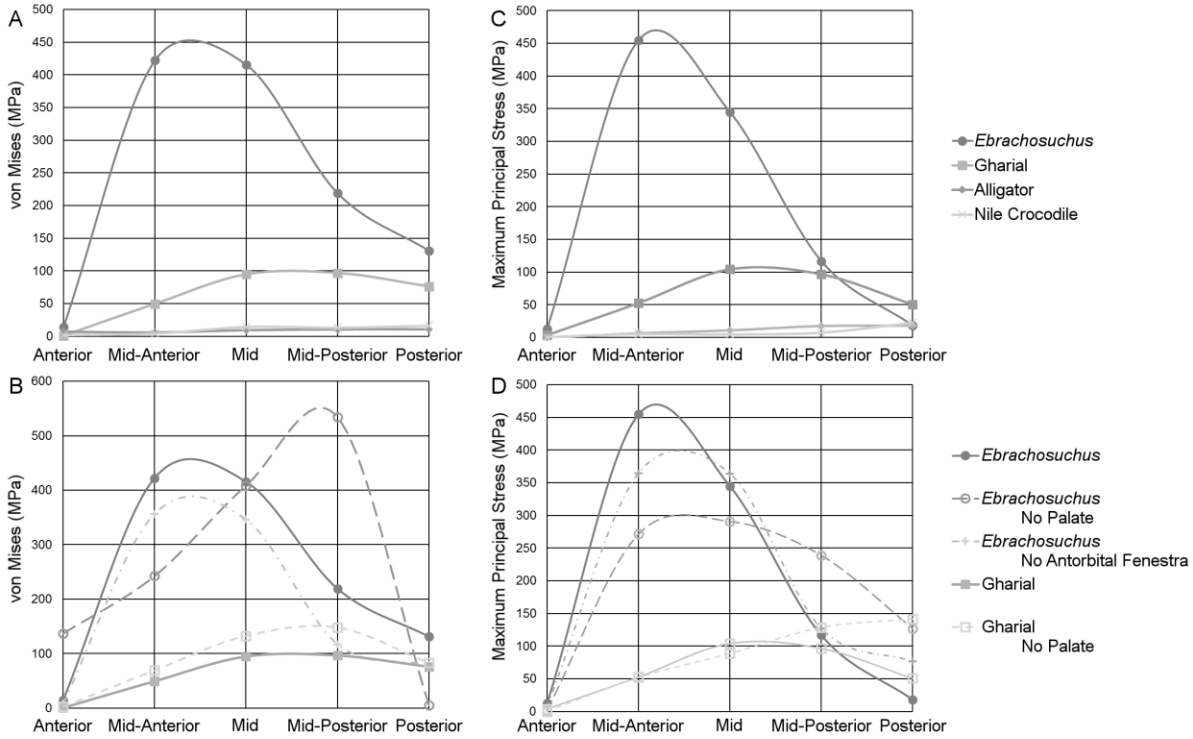

528

529 **Figure 8**. **Stress values from selected ventral nodes.** Comparison of stress values between the finite
530 element models of the crocodilians and *Ebrachosuchus* taken under a bilateral load at the anterior most
531 position. Data was taken at points along the ventral surface of each skull through the region of maximum
532 stress. Similar trends are seen in both von Mises and maximum principal stress values. Removal of the
533 palate in both the gharial and *Ebrachosuchus* increase the observed peak von Mises values while closing
534 the antorbital fenestra in *Ebrachosuchus* consistently decreases the observed von Mises values; maximum
535 principal stress shows less consistent patterns between the original and manipulated geometries. The
536 bilateral and unilateral data show the same trends between specimens.

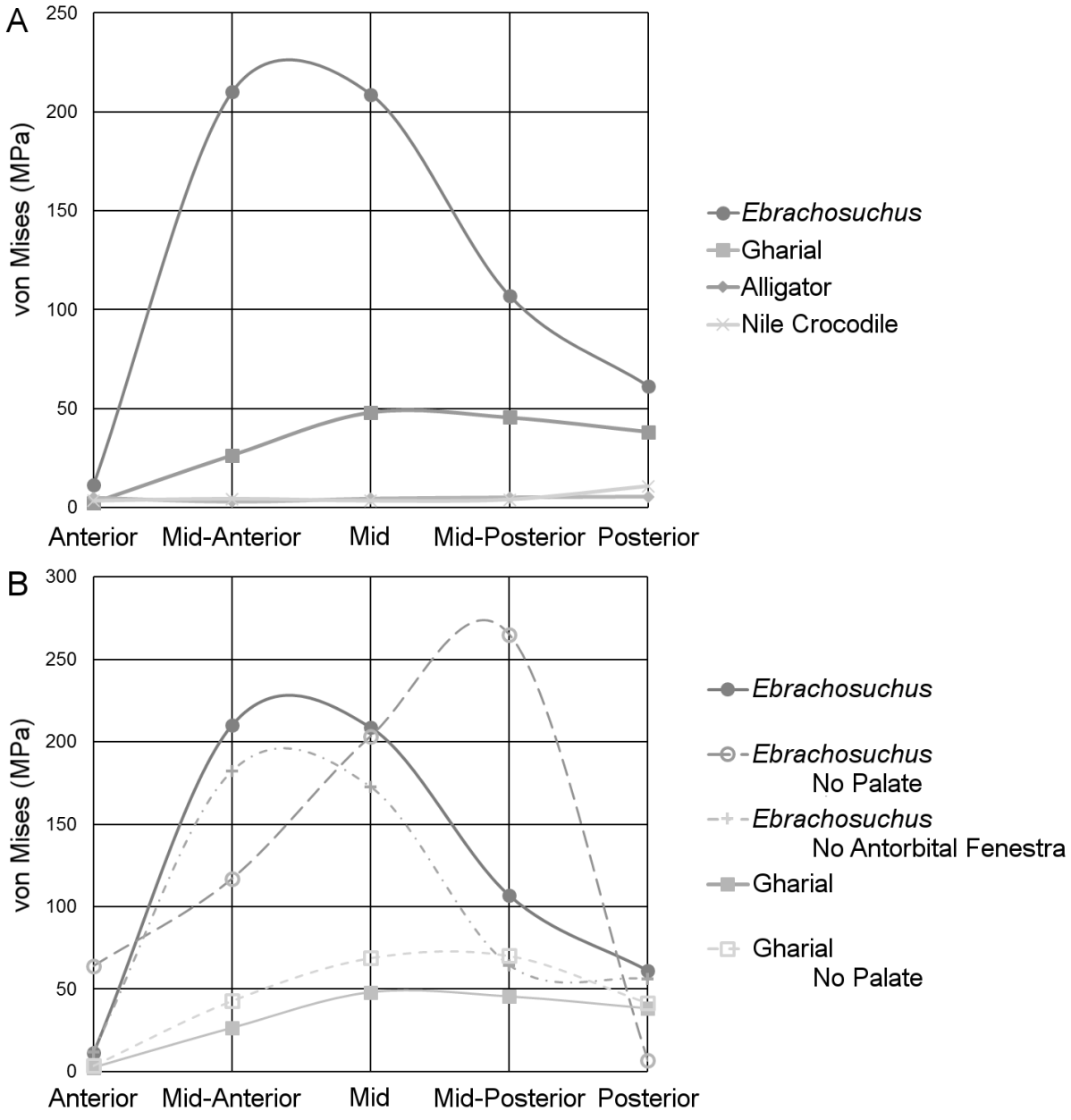

Figure 9. Stress values of head-shaking and theoretical skull morphologies. Stress values taken from the anterior head-shaking load. The same trends are seen in this data (A) and the bilateral (Fig. 5) and unilateral data. However, comparisons between the original and manipulated morphologies (B) show slight relative differences in the posterior of the skulls. Due to the limited number of nodes queried and differences in locations, these values reflect local effects; compare Figures 8 and 9 with Figures 10 and 11.

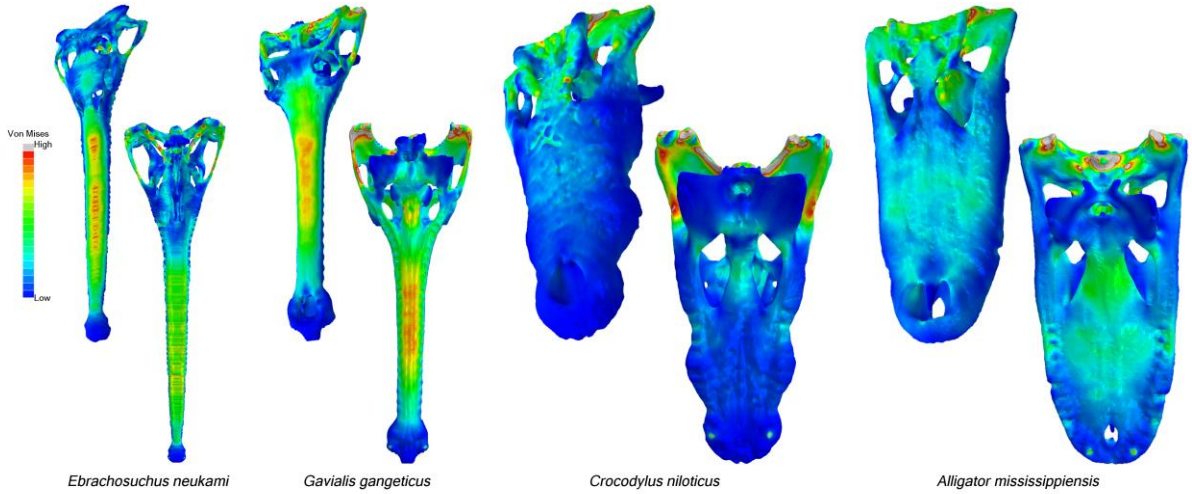

Figure 10. **Skull stresses during bilateral biting.** Results of the finite element analysis. All models show the distribution of von Mises stress about the skull under bilateral loading conditions with the load placed at the anterior end of the rostrum. Both *Ebrachosuchus* and the gharial show high stress along the rostrum with the highest stress forming along the midline, near the center of the rostrum. Results of the unilateral loading conditions show similar results.

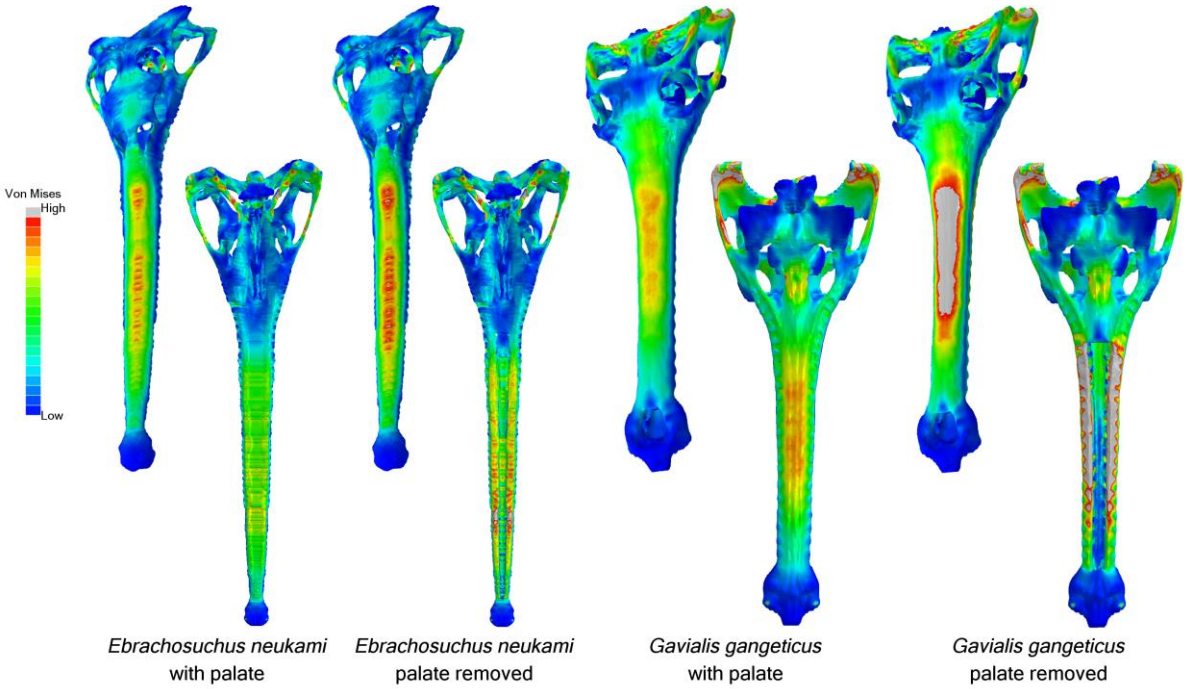

549

550 **Figure 11. Comparisons of skull stresses between the original and theoretical skull morphologies.**
551 Comparison of the palate and no palate models for *Ebrachosuchus* and the gharial. The palates were
552 manually removed from the 3D surface files. Loading conditions are the same as in Figure 3. Removal of
553 the palates increases the magnitude of stress that develops along the rostrum.

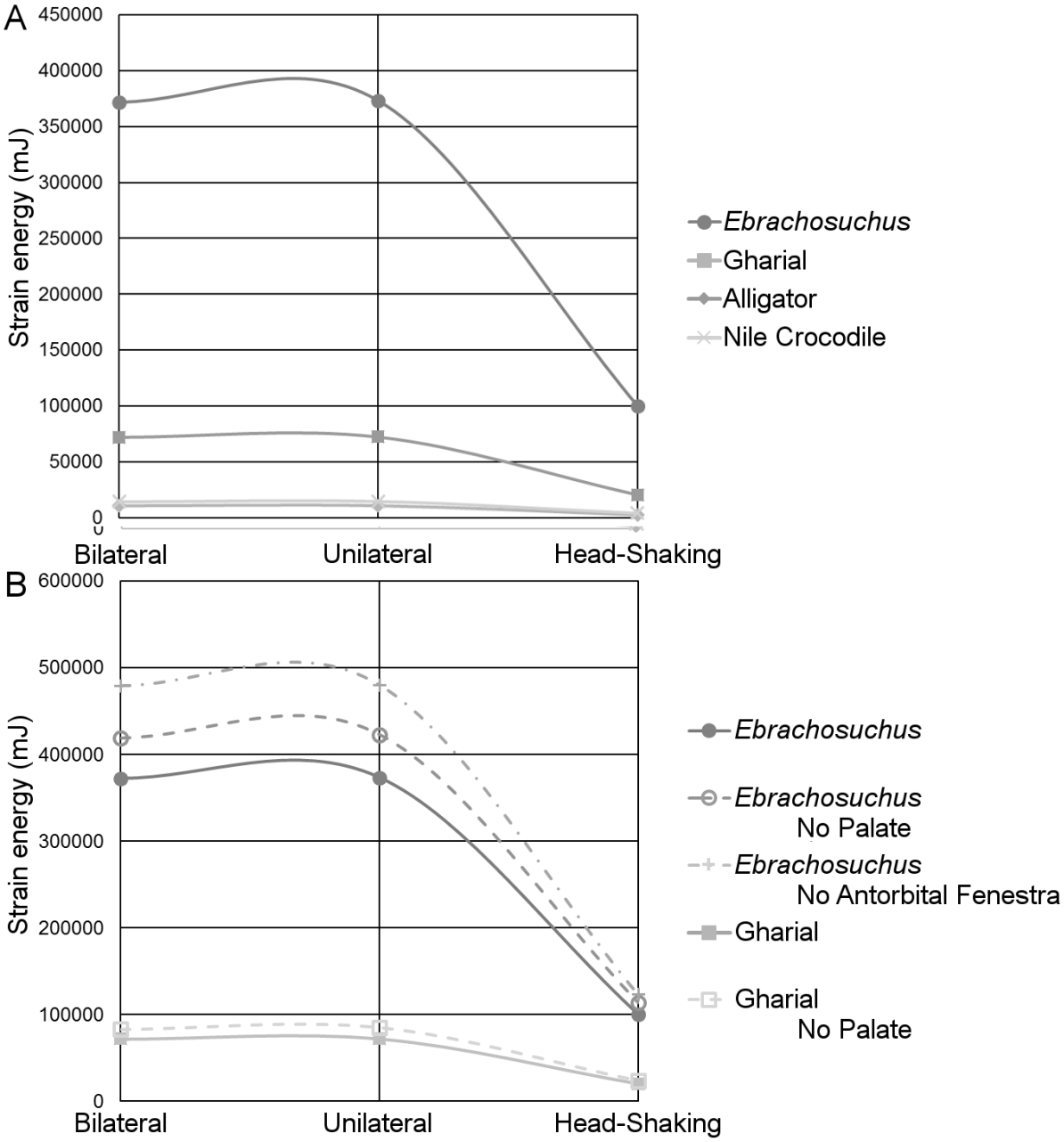

554

555 **Figure 12. Strain energy values under all loading conditions.** Total strain energy values for all three
556 loading conditions applied to the anterior loading position. Strain energy has been scaled to volume. All
557 morphological manipulations of the skulls of the gharial and *Ebrachosuchus* increase the calculated strain
558 energy (B).